Optimal Efficiency Control in a Wind System With Doubly Fed Induction Generator

Nektarios Karakasis, Evangelos Tsioumas, Nikolaos Jabbour, Ali M. Bazzi, *Senior Member, IEEE*, and Christos Mademlis, *Senior Member, IEEE*

***Abstract*—This paper proposes an optimal efficiency control scheme for a wind system with doubly fed induction generator (DFIG). The suggested control scheme combines loss minimization (LM) in the DFIG and maximum power point tracking (MPPT) in the wind turbine and therefore maximum electrical energy generation, by the same wind energy potential, is achieved. Moreover, since the cut-in wind speed is reduced, extension of the exploitable wind speed range toward the lower speed region is attained. The LM is achieved by properly controlling the flux-linkage of the DFIG with respect to the stator current and the MPPT is accomplished by regulating the rotor speed through the rotor current. The parameters of the LM and MPPT controllers can be determined experimentally, and thus, the knowledge of the wind energy conversion system (WECS) model is not required. For the implementation of the proposed control strategy, a new structure of the WECS has been adopted. However, the hardware requirements of the WECS and considerably the cost have not been considerably affected compared to the conventional configuration. Selective simulation and experimental results are presented to validate the effectiveness of the proposed control strategy and demonstrate the operational improvements.**

***Index Terms*—Doubly fed induction generator (DFIG), efficiency increase, power loss reduction, wind turbine, wind system.**

I. Introduction

IN RECENT years, the number of wind systems with doubly fed induction generators (DFIGs) connected to the national networks has considerably increased, due to their advantageous characteristics against the main competitor which is the permanent magnet synchronous generator (PMSG) [1]. Specifically, a wind energy conversion system (WECS) with DFIG attains lower requirements for power converter capacity, flexible regulation of active and reactive powers since they can be provided by two parallel paths from the stator and rotor sides, higher power quality since the greater amount is provided by the stator that is directly connected to the grid without a power converter being interposed, and also independence from permanent magnets

Manuscript received November 22, 2017; revised February 14, 2018; accepted March 29, 2018. Date of publication April 4, 2018; date of current version November 19, 2018. Recommended for publication by Associate Editor Dr. A. K. Gupta. *(Corresponding author: Dr. Christos Mademlis.)*

N. Karakasis, E. Tsioumas, N. Jabbour, and C. Mademlis are with the School of Electrical and Computer Engineering, Aristotle University of Thessaloniki, Thessaloniki GR-54124, Greece (e-mail:

a DFIG connected to a common dc-link for the stator and rotor side has been proposed in [22]. A technique that provides maximum active and reactive power control in a WESC with a matrix-converter fed DFIG has been presented in [23], which is based on the proper share between the DFIG stator and the input terminal of the matrix converter. Control schemes for both LM and maximum power point tracking (MPPT) in a DFIG wind system have been proposed in [24] and [25]; however, an additional power converter is applied in the stator side to control the flux-linkage, and also, the effectiveness of the proposed system has been verified only by simulations. The efficiency improvement in a DFIG that operates in a rotor-tied configuration, while the control is performed by the stator side, has been examined in [26]. Finally, an MPPT technique for WECS with DFIG has been proposed in [27] and the effect of rotor excitation voltage on the steady-state stability and maximum output power of a DFIG has been examined in [28].

From the above, it is concluded that the problem of efficiency optimization in WECS with DFIG is an open issue and a new control scheme based on flux-weakening is required that does not affect the benefits of the DFIG compared to the other generator types and does not increase the hardware requirements of the WECS. Since the stator of the DFIG is directly connected to the grid, the only available option to regulate the flux-linkage is provided by the rotor side converters. Therefore, the conventional structure of the WECS should be properly reconfigured, but without considerably increasing the hardware requirements and consequently, without considerably affecting the cost of the system.

Therefore, the aim of this paper is to present a combined control system for LM in the DFIG and MPPT in the wind turbine of a WECS in order to increase the electric energy that can be generated by the same wind energy potential. Also, a decrease in the cut-in wind speed and therefore expansion of the exploitable wind speed range toward the low wind speed region can be accomplished. The proposed optimal efficiency control technique is developed for power factor equal to a unit at the point of common coupling to the grid, since it is more preferable in the vast majority of wind systems. For the implementation of the proposed optimal efficiency control scheme, the knowledge of the WECS model is not required, since the parameters of the controllers can be determined experimentally. Several simulation and experimental results are presented in order to demonstrate the feasibility and the operational improvements of the new control system. Specifically, simulation results are obtained by a high power wind system of 1.6 MW and experimental results are obtained by a low power scaling laboratory emulation wind system of 5.5 kW.

II. Proposed System Topology

In order to implement the optimal efficiency control technique, a new structure for the WECS with DFIG is adopted, that is illustrated in Fig. 1(a) and can be compared with the conventional structure of Fig. 1(b). As can be seen, a system of two back-to-back converters at the rotor side (generator side converter, GeSC, and grid side converter, GrSC) of the same power capacity as in the conventional configuration is used in the new structure. Also, a crowbar resistance to dissipate the excess electrical energy and a battery storage system to both smooth the generated energy and keep the dc-link voltage constant are utilized in both configurations [29].

The dual-primary single-secondary grid transformer of the conventional system [see Fig. 1(b)] has been replaced by a simpler single-primary single-secondary transformer in the new system [see Fig. 1(a)]. The isolation between the stator and rotor of the DFIG and the adaptation of the rotor voltage level is accomplished by using another single-primary single-secondary rotor transformer. An *LCL* filter is also utilized [30], [31], as in the conventional system of Fig. 1(b); however, it is of lower inductance, since the filtering is assisted by the inductances of the rotor transformer.

Comparing the two configurations, it is resulted that two new transformers are introduced in the optimal efficiency system of Fig. 1(a) and they replace the grid transformer of the conventional system of Fig. 1(b). Both the new rotor and grid transformers of Fig. 1(a) have single-primary single-secondary windings and also, the rotor transformer is of lower nominal power, since it is referred to the low nominal power of the rotor side conversion system. On the other hand, the grid transformer of the conventional system of Fig. 1(b) has dual-primary single-secondary windings with nominal power equal to nominal power of the WECS. Thus, two lower cost transformers in the new system (i.e., the rotor transformer due to both the simpler construction and the lower nominal power and the grid transformer due to the simpler construction) have replaced the higher cost grid transformer of the conventional system. Furthermore, the *LCL* filter of the new system has lower inductance and therefore, less windings compared to the conventional system, since the filtering is assisted by the inductances of the rotor transformer. Considering the above, it is concluded that the implementation of the WECS with the new topology does not affect considerably the cost compared with the conventional topology. On the other hand, the new WECS-DFIG structure of Fig. 1(a) holds the advantages of the conventional system against the PMSG (i.e., stator tied to the grid, lower requirements for power converter capacity, and flexible regulation of active and reactive powers from the stator and rotor energy paths as well as independence from PMs).

The above cost comparison between the two configurations has been conducted on the basis of the factors of power capacity and construction of the power components that mainly affect the cost of a power system. A quantified cost comparison is out of the scope of the paper, since it requires a detailed economic analysis, and also, it is highly dependent on the market prices of the components and the specific technical characteristics of the WECS.

In addition to the cost comparison, it is important to examine the components that have been changed in the new topology from the power loss point of view. Comparing the rotor and grid transformers of Fig. 1(a) with the grid transformer of Fig. 1(b), it is concluded that the power losses are increased by the iron loss and the copper loss of one side windings of the rotor transformer. However, the additional iron loss of Fig. 1(a) is lower than the

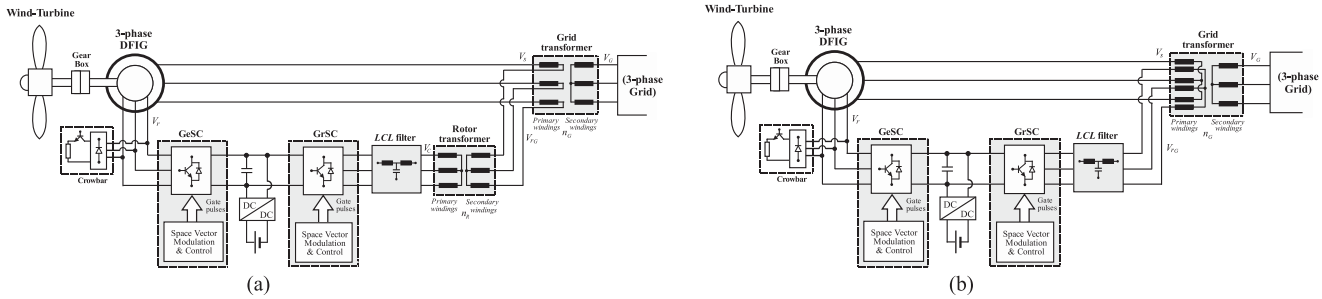

Fig. 1. Comparison of the structure of a variable speed WECS with DFIG. (a) Proposed optimal efficiency system. (b) Conventional system.

iron loss of the grid transformer of Fig. 1(b), since the rotor transformer has lower operating voltage. Also, lower iron and copper losses are observed in the *LCL* filter of Fig. 1(a) due to the less windings and lower operating voltage compared to the *LCL* filter of the conventional WECS in Fig. 1(b). It should be noted that, since the above comparison is highly dependent on the technical characteristics of the WECS's components, it is not possible to come to an assured conclusion which can hold for all WECS with DFIG.

The rated power of the GeSC and GrSC of the new WECS topology of Fig. 1(a) is almost the same as the conventional system of Fig. 1(b), and also, almost the same power loss is observed in GeSC and GrSC for both system topologies. The key point of the new structure [see Fig. 1(a)] is that each of the primary winding of the grid transformer connects, in its two sides, the stator of the DFIG and the output of the GrSC through the rotor transformer and the *LCL* filter. Thus, the stator voltage and consequently the flux-linkage of the DFIG can be regulated by controlling the output voltage of GrSC, while the voltage at the WECS side of the grid transformer remains constant, as imposed by the grid. Therefore, flux weakening control and, therefore, LM in the DFIG can be attained through the proper control of the GrSC by regulating the stator voltage, and MPPT in the wind turbine is accomplished through the proper control of the GeSC by adjusting the rotor speed.

At the event of a grid fault in the new topology in Fig. 1(a), since the primary winding of the grid transformer is in series between the stator and rotor sides of the DFIG, the stator voltage of the DFIG initially becomes lower compared to the reduced stator voltage that is caused by a similar grid fault in the conventional system of Fig. 1(b). However, since the stator voltage of the DFIG is regulated by the LM controller of the GrSC output voltage, the fault can be more effectively mitigated compared to the conventional system of Fig. 1(b) in which the stator faces the exact low voltage caused by the fault because the stator voltage is not controlled. From the above, it is concluded that the proposed topology of Fig. 1(a) has enhanced fault-ride-through capability against a grid fault or disturbance in the stability standpoint for both the stator (through the proper control of the GrSC) and the rotor side of the DFIG (through the proper control of the crowbar and the battery) compared with the conventional topology of the Fig. 1(b) in which, only the proper control of the crowbar and the battery can provide fault-ride-through capability for the whole WECS.

TABLE I
COMPARISON BETWEEN OPTIMAL WITH CONVENTIONAL WESC CONFIGURATION

	OPTIMAL EFFICIENCY WECS		CONVENTIONAL WECS	
COST	ROTOR TRANSFORMER	Lower nominal power Single winding configuration	GRID TRANSFORMER	WECS nominal power Multiple winding configuration
	GRID TRANSFORMER	WECS nominal power Single winding configuration		
	LCL FILTER	Lower inductance and thus, less windings	LCL FILTER	Higher inductance and thus, full windings
	POWER CONVERTERS	Rotor-side nominal power	POWER CONVERTERS	Rotor-side nominal power
POWER LOSS	ROTOR TRANSFORMER	Lower iron loss Copper loss in 2 windings	GRID TRANSFORMER	Higher iron loss Copper loss in 3 windings
	GRID TRANSFORMER	Higher iron loss Copper loss in 2 windings		
	LCL FILTER	Lower iron loss (due to lower operating voltage Lower copper loss (due to less windings)	LCL FILTER	Higher iron loss Higher copper loss
	POWER CONVERTERS	Same power loss	POWER CONVERTERS	Same power loss
FAULT-RIDE-THROUGH	Enhanced fault-ride-through capability, since the stator voltage of the DFIG is controlled by the GrSC		Only by the proper control of the crowbar and the GeSC	

The conclusions of the comparison of the new WECS topology with the conventional one with regard to the cost, power loss, and fault-ride-through capability are reported in Table I.

III. POWER LOSS MODEL OF THE DFIG

The aerodynamic power absorbed by a wind turbine is

$$P_{\text{wt}} = 0.5\rho\pi R^2 C_p u^3 \tag{1}$$

where ρ is the air density, C_p is the turbine power coefficient, *u* is the wind speed, and *R* is the blades radius. For a given blade pitch angle β, the optimal tip-speed ratio λ_{opt} is constant for all MPPs and, thus, the optimum rotor angular velocity is

$$\omega_{\text{wt}_{\text{opt}}} = \frac{\lambda_{\text{opt}} u}{R}. \tag{2}$$

Since a gear box is used, the turbine speed ω_{wt} and the turbine torque $\tau_{\text{wt}} = P_{\text{wt}}/\omega_{\text{wt}}$ are adapted to the generator level on the basis of the gear ratio *n,* and thus, the generator mechanical speed and torque are $\omega_m = n\,\omega_{\text{wt}}$ and $T_m = T_{\text{wt}}/n$, respectively.

For having decoupling control in a DFIG, the stator flux-linkage is aligned to the *d*-axis ($\psi_s = \psi_{ds}$) and, therefore

$$\psi_{qs} = 0 \tag{3}$$

Since

$$\psi_{qs} = L_{ls} I_{qs} + L_m \left(I_{qs} + I_{qr}\right) \tag{4}$$

yields

$$I_{qr} = -\frac{L_m + L_{ls}}{L_m} I_{qs} \tag{5}$$

where ψ_s is the stator flux-linkage, ψ_{ds} and ψ_{qs} are the *d*- and *q*-axis stator flux-linkages, respectively, and L_m and L_{ls} are the magnetizing and stator leakage inductances, respectively.

The reactive power at the stator of the DFIG is given by

$$Q_s = 1.5\left(I_{ds}V_{qs} - I_{qs}V_{ds}\right) \tag{6}$$

where

$$V_{ds} = R_s I_{ds} + \omega_e \psi_{qs} \tag{7}$$

$$V_{qs} = R_s I_{qs} + \omega_e \psi_{ds}. \tag{8}$$

Due to (3), (6) results in

$$Q_s = 1.5 I_{ds} \psi_{ds} \omega_e. \tag{9}$$

As can be seen in Fig. 1(a), the primary windings of the grid transformer are in the middle of the series connection path between the stator of DFIG and the secondary windings of the rotor transformer. Thus, since the power factor at the point of common coupling to the grid is equal to 1, the reactive power at the stator of the DFIG is 0 ($Q_s = 0$). Thus, the reactive power for the DFIG is supplied by the rotor through the GeSC, while the reactive power for the rotor and grid transformers as well as the *LCL* filter is provided by the GrSC. Considering the above and also that ψ_{ds} cannot be 0, from (9), it is concluded that

$$I_{ds} = 0 \tag{10}$$

and using (3) and (10) in (7), results

$$V_{ds} = 0. \tag{11}$$

Since

$$\psi_{ds} = L_{ls} I_{ds} + L_m\left(I_{ds} + I_{dr}\right) \tag{12}$$

and due to (10), results $\psi_{ds} = L_m I_{dr}$. Therefore, the airgap flux-linkage of a DFIG is given by

$$\psi_m = L_m I_{dr} \tag{13}$$

and thus

$$I_{dr} = \frac{\psi_m}{L_m}. \tag{14}$$

The electric power loss of a DFIG is given by

$$P_l = 1.5R_s\left(I_{ds}^2 + I_{qs}^2\right) + 1.5R_r\left(I_{dr}^2 + I_{qr}^2\right) + c_{Fe_s}\omega_e^2\psi_m^2 + c_{Fe_r}\left(\omega_e - \omega_r\right)^2\psi_m^2 + c_{str}\omega_e^2\left(I_{ds}^2 + I_{qs}^2\right) \tag{15}$$

where R_s and R_r are the stator and rotor resistances, respectively, c_{Fe_s} and c_{Fe_r} are the stator and rotor core loss coefficients, respectively, c_{str} is the stray loss coefficient, and ω_r is the rotor electrical speed ($\omega_r = p\omega_m$, where p is the number of pole pairs). It should be noted that the mechanical loss is not affected by the flux-weakening. The stator and rotor iron losses are due to hysteresis and eddy currents. The formula that the iron losses vary with the square of both frequency and flux is resulted by the modified Steinmetz approximation, that is, the iron loss in an electrical machine can be considered in the equivalent circuit by an ohmic resistance in parallel to the magnetizing inductance [32], [33].

By substituting (5), (10), and (14) in (15), the electric power loss of the DFIG can be rewritten as follows:

$$P_l = aI_{qs}^2 + b\psi_m^2 \tag{16}$$

where

$$a = 1.5R_s + 1.5R_r\left(\frac{L_m + L_{ls}}{L_m}\right)^2 + c_{str}\omega_e^2 \tag{17}$$

$$b = 1.5\frac{R_r}{L_m^2} + c_{Fe_s}\omega_e^2 + c_{Fe_r}\left(\omega_e - \omega_m\right)^2. \tag{18}$$

The electromagnetic torque in a DFIG is given by

$$T_e = 1.5p\left(\psi_{ds}I_{qs} - \psi_{qs}I_{ds}\right) \tag{19}$$

and due to (3) yields

$$T_e = 1.5p\,\psi_m I_{qs}. \tag{20}$$

IV. Optimal Efficiency in a WECS With DFIG

The optimal efficiency in a WECS with DFIG can be achieved by LM in the DFIG and MPPT in the wind turbine.

A. Optimal Efficiency in a DFIG

For a given rotor speed and in steady-state operation, the electric power loss of a DFIG can be minimized with respect to ψ_m by

$$\left.\frac{\partial P_l}{\partial \psi_m}\right|_{\omega_r = \text{const.}} = 0 \tag{21}$$

and considering (16) results in

$$aI_{qs}\frac{\partial I_{qs}}{\partial \psi_m} + b\psi_m = 0. \tag{22}$$

Since for a given rotor speed, the electromagnetic torque of a DFIG is constant

$$\left.\frac{\partial T_e}{\partial \psi_m}\right|_{\omega_r = \text{const.}} = 0 \tag{23}$$

from (20), we have

$$\frac{\partial I_{qs}}{\partial \psi_m} = -\frac{I_{qs}}{\psi_m}. \tag{24}$$

Substituting (24) in (22) results in

$$\psi_m = I_{qs}\sqrt{\frac{a}{b}} \tag{25}$$

and using (17) and (18), the optimal airgap flux-linkage of the DFIG that provides LM is given by

$$\psi_{m\,\text{opt}} = I_{qs}G_s\sqrt{\frac{1 + \omega_e^2 T_A}{1 + \omega_e^2 T_B + \left(\omega_e - \omega_m\right)^2 T_C}} \tag{26}$$

where

$$G_s = \sqrt{L_m^2\frac{R_s}{R_r} + \left(L_m + L_{ls}\right)^2} \tag{27}$$

$$T_A = \frac{c_{str} L_m^2}{1.5 R_s L_m^2 + 1.5 R_r (L_m + L_{ls})^2} \tag{28}$$

$$T_B = \frac{c_{Fe_s} L_m^2}{1.5 R_r} \tag{29}$$

and

$$T_C = \frac{c_{Fe_r} L_m^2}{1.5 R_r}. \tag{30}$$

Since the power factor at the point of common coupling is equal to 1 and due to (10), the relationship between the q-axis components of the DFIG stator voltage V_{qs} and the GrSC output voltage $V_{q\text{Cov}}$ is given by

$$V_{qs} - \frac{V_{q\text{Cov}}}{n_R} = n_G V_G + I_{qs} R_{Tr} \tag{31}$$

where n_G and n_R are the turns-ratios of the grid and rotor transformers, respectively, R_{Tr} is the equivalent ohmic resistance of the rotor transformer and the *LCL* filter, and V_G is the grid voltage. From (31) and using (8), (26), and (27), the optimal condition for the $V_{q\text{Cov}}$ that provides LM in the DFIG is given by

$$V_{q\text{Cov}_{\text{opt}}} = I_{qs} n_R \left[\Delta R + \omega_e G_s \sqrt{\frac{1 + \omega_e^2 T_A}{1 + \omega_e^2 T_B + (\omega_e - \omega_m)^2 T_C}} \right] - n_R n_G V_G \tag{32}$$

where

$$\Delta R = R_s - R_{Tr}. \tag{33}$$

Due to (10) and (11), the d-axis component of the GrSC output voltage $V_{d\text{Cov}}$ is given by

$$V_{d\text{Cov}} = \omega_e L_{Tr} I_{qs} \tag{34}$$

where L_{Tr} is the equivalent inductance of the rotor transformer and the *LCL* filter.

B. MPPT in a Wind Turbine

The MPPT is attained with maximum aerodynamic coefficient $C_{p_{\text{opt}}}$ and, thus, from (1) and (2) and considering $\omega_m = n\,\omega_{wt}$ and $T_m = T_{wt}/n$ (where n is the gear ratio), the turbine torque in the generator shaft is

$$T_{m_{\text{opt}}} = \frac{\rho \pi R^5}{2 n^3 \lambda_{\text{opt}}^3} C_{p_{\text{opt}}} \omega_m^2. \tag{35}$$

Since the DFIG electromagnetic torque is

$$T_{e_{\text{opt}}} = T_{wt_{\text{opt}}} - T_{m_l} \tag{36}$$

where T_{m_l} is the mechanical loss torque that is proportional to the second power of the rotor speed [34], [35], using (35) results in

$$T_{e_{\text{opt}}} = \left[\frac{\rho \pi R^5}{2 n^3 \lambda_{\text{opt}}^3} C_{p_{\text{opt}}} - c_{ml} \right] \omega_m^2 \tag{37}$$

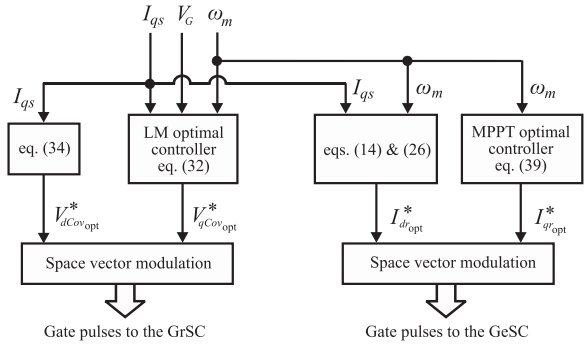

Fig. 2. Control scheme for the optimal efficiency WECS with DFIG.

where c_m is the mechanical loss coefficient. Taking into account (20), the q-axis stator current that provides MPPT in the wind turbine is given by

$$I_{qs} = \left(\frac{\rho \pi R^5 C_{p_{\text{opt}}} - 2 c_{ml} n^3 \lambda_{\text{opt}}^3}{3 p n^3 \lambda_{\text{opt}}^3} \right) \frac{\omega_m^2}{\psi_m}. \tag{38}$$

Then, by substituting (26) in (38) and using (5), the optimal I_{qr} current condition is given by

$$\left| I_{qr_{\text{opt}}} \right| = \omega_m \frac{G_r}{\sqrt{G_s}} \left(\frac{1 + \omega_e^2 T_B + (\omega_e - \omega_m)^2 T_C}{1 + \omega_e^2 T_A} \right)^{1/4} \tag{39}$$

where

$$G_r = \frac{L_m + L_{ls}}{L_m} \sqrt{\frac{\rho \pi R^5 C_{p_{\text{opt}}} - 2 c_{ml} n^3 \lambda_{\text{opt}}^3}{3 p^3 n^3 \lambda_{\text{opt}}^3}}. \tag{40}$$

Although, the above MPPT control method implemented by the optimal condition (39) has been selected in this paper, the proposed LM control technique for the DFIG that is realized by the WECS structure of Fig. 1(a) can cooperate with any of the other MPPT control methods proposed in the technical literature, such as search control [34], fuzzy-logic control [36], and neural networks control methods [35].

C. WECS Optimal Efficiency Control

To attain maximum efficiency of the whole WECS, both LM and MPPT optimal conditions of (32) and (39), respectively, should be satisfied simultaneously. Specifically, the LM in the DFIG is attained through the optimal condition (32) that determines the optimal $V_{q\text{Cov}}$ voltage and needs the measurements of the I_{qs} current, grid voltage V_G, and rotor speed ω_m. The MPPT in the wind turbine is accomplished by the condition (39) that determines the optimal I_{qr} current and needs the measurement of the rotor speed ω_m. The LM is attained through the GrSC and the MPPT is realized by the GeSC.

V. Implementation of the Optimal Efficiency Control in a WECS With a DFIG

The control scheme that provides LM in the DFIG and MPPT in the wind turbine and, therefore, optimal efficiency in the whole WECS, is illustrated in Fig. 2. The $V_{q\text{Cov}_{\text{opt}}}$ can take either positive or negative values depending on the wind conditions.

Specifically, positive $V_{q\text{Cov}_{\text{opt}}}$ corresponds to the energy flow from the grid to the rotor conversion system and vice-versa for negative $V_{q\text{Cov}_{\text{opt}}}$.

As can be seen in Fig. 2, the LM and the MPPT are applied in two different power converters but they have common inputs I_{qs} current and ω_m. The LM is accomplished through the proper control of the *q*-axis output voltage of the GrSC and the MPPT is attained by controlling the *q*-axis rotor current of the DFIG through the GeSC. The other two vector components of the above variables regulate the reactive power of the WECS. Specifically, the *d*-axis output voltage of the GrSC is determined by (34) and attains zero reactive power at the point of common coupling to the grid. The *d*-axis rotor current of DFIG is determined by (14) and regulates the required reactive power to the DFIG by considering the optimal flux linkage that is determined by (26).

Both the LM and the MPPT controllers operate within the acceptable rotor speed range around the synchronous speed of a WECS, as per [37] and [38]. Specifically, the MPPT controller provides the optimal rotor speed, while the LM determines the optimal flux-linkage of the DFIG. Therefore, the proper operation of the WECS within the acceptable rotor speed range is the responsibility of the MPPT controller, while the LM controller ensures optimal efficiency in the WECS by considering the rotor speed ω_m and the I_{qs} current that are regulated by the MPPT control.

The battery storage system has a dual role in the new optimal efficiency controlled WECS. Specifically, it provides power and energy smoothing, and also, keeps constant the dc-link voltage. Thus, part of the energy that flows at the rotor side of the DFIG may be temporarily stored/released in the battery depending on the wind conditions and, therefore, a technoeconomic study should be conducted in order to decide for the proper energy storage capacity of the battery for each WECS installation.

The turns-ratio n_R of the rotor transformer is decided according to the desired voltage level of the rotor side power conversion system. The turns-ratio n_G is decided by taking into account the energy storage capacity of the dc-link battery, the DFIG power loss model, and the wind energy potential of the installation area. Specifically, if n_G is high, the $V_{q\text{Cov}_{\text{opt}}}$ takes negative values in most of the wind speed range. In this case, the energy mainly flows from the GrSC to the grid and, thus, the battery at the rotor dc-link operates in discharging mode for most of the wind speed range. On the contrary, if n_G is relatively low, $V_{q\text{Cov}_{\text{opt}}}$ takes positive values, and thus, the battery operates in charging mode for most of the wind speed range. Therefore, a case study should be conducted in order to determine the proper n_G turn-ratio that can statistically ensure the lowest energy storage capacity of the battery for both guaranteeing effective optimal efficiency control and power/energy smoothing at the dynamic operation of the WECS. If n_s is the ratio between nominal stator voltage of the DFIG V_s and grid voltage V_G, typical values of n_G are $0.55\,n_s$ to $0.85\,n_s$.

For the implementation of the LM and MPPT controllers, the knowledge of the parameters G_s, T_A, T_B, and T_C and ΔR of the (32) and G_r of the (40) are required. The ΔR is measured by an ohmmeter, while rest of the parameters can be determined by the following experimental procedure that can be conducted in a laboratory emulation wind system.

1) The wind turbine mechanical torque is 15%–20% of the nominal value. The DFIG rotates at 70%–80% of the synchronous speed and the output power of the WECS to the grid is measured. Since $\omega_e - \omega_m$ is high, the condition (32) becomes

$$V_{qC_{\text{opt}}} \simeq n_R I_{qs} \left(\Delta R + \omega_e G_s\right) - n_R n_G V_G. \qquad (41)$$

$V_{q\text{Cov}}$ is adjusted so that maximum electric power is provided to the grid and the gain G_s is determined from (41).

2) The rotor speed increases to 90%–95% of the synchronous speed and $V_{q\text{Cov}}$ is adjusted so that maximum electric power is provided to the grid. The same is repeated for rotor speeds 105%–110% and 125%–130% of the synchronous speed. By substituting the above three sets of measurements in (32) and using the value of G_s determined by the previous step, a system of three equations with unknown parameters T_A, T_B, and T_C is obtained and then by solving it, the above parameters can be determined.
3) Steps 1) and 2) are repeated until the desired accuracy is accomplished.

The gain G_r of the MPPT controller of (40) can be experimentally determined through the adaptive neuro-fuzzy logic control technique proposed in [39]. The experimental procedure is realized during the real operation of the WECS. Specifically, the DFIG is operated with the LM controller as described by the condition (32). For any given wind speed, the I_{qr} is adjusted through the adaptive neuro-fuzzy logic control algorithm for accomplishing MPPT and then the G_r parameter is determined by the condition (39). Due to the degradation that may occur by the aging of the mechanical parts of the turbine, the above experimental procedure should be repeated periodically.

As can be observed in (27), the gain G_s depends on the static and ohmic resistances and, thus, it may vary with temperature. However, since ohmic resistances are both in the numerator and the denominator of the first term of (27), their variation with temperature is counterbalanced and, therefore, the gain G_s remains almost unaffected. For similar reasons, although the parameters T_A, T_B, and T_C depend on the stator and rotor ohmic resistances, (26) is not considerably affected because T_A is in the numerator, while T_B and T_C are in the denominator and, therefore, their variation is compensated. Also, ΔR of (33) is not considerably affected by the temperature variation because it is a subtraction between two resistances and, therefore, the variation of the one is compensated by the variation of the other.

The gain G_s and the parameters T_A, T_B, and T_C depend on the L_m and, thus, may vary with the magnetic saturation. However, L_m is both in numerator and denominator of T_A and, therefore, the variation of T_A with saturation is counterbalanced. Also, although G_s, T_B, and T_C decrease with the increase of saturation, the $V_{q\text{Cov}}$ remains almost unaffected because G_s is in the numerator, while T_B and T_C are in the denominator of the second term of (32). For similar reasons, G_r is almost unaffected by the magnetic saturation, since L_m is both in numerator and denominator.

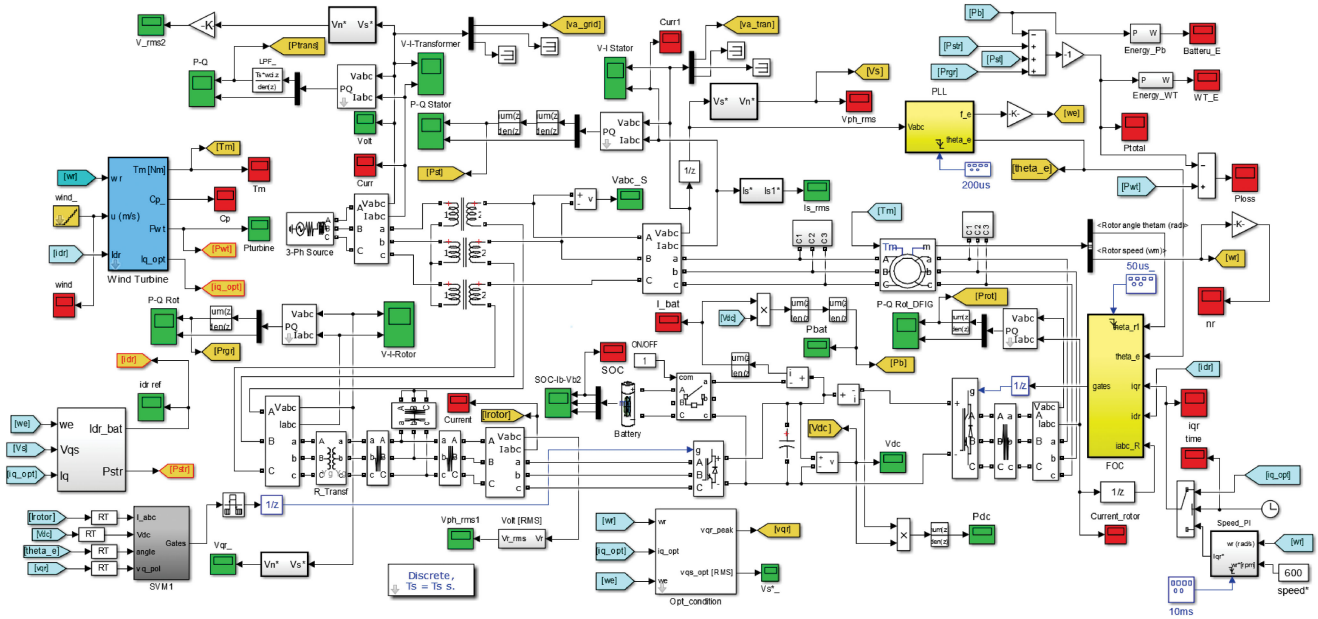

Fig. 3. Block diagram of the MATLAB/Simulink model of a 1.6-MW WECS with DFIG.

It should be noted that some variations for the LM controller parameters are acceptable because the power loss curves [see Fig. 4(a)] are smooth and flat around the minimum and thus, LM is reached for a wide range of $V_{q\mathrm{Cov}}$. Similar holds for the MPPT control [see Fig. 4(b)].

VI. Simulation Results

The proposed control scheme was tested with simulations on a high-power WECS with DFIG of 1.6 MW and experimentally on a low power scaling system of 5.5 kW.

The MATLAB/Simulink program has been used for the simulation analysis [40]. The block diagram of the simulation model of the 1.6-MW WECS with DFIG is illustrated in Fig. 3. The parameters of the WECS, the DFIG, the rotor and grid transformers, the *LCL* filter, and the optimal controllers are reported in Table II. The WECS operation initiates by having the LM and MPPT controllers inactive and the DFIG operates as a motor by means of a PI controller. Then, the DFIG accelerates and when the rotor speed reaches 600 r/min, the LM and MPPT controllers are activated and, thus, the WECS turns to the normal operation. The field-oriented control with space vector modulation is applied in the two back-to-back converters of the rotor side DFIG with sampling time for both converters equal to 0.2 ms. The reference d- and q-axes components of the GeSC's rotor current and GrSC's output voltage are determined by the block diagram of Fig. 2 and the sampling time of the LM and MPPT optimal controllers is 2 ms. A battery stack with a rated capacity of 70 A is used at the dc-link. The power factor at the point of common coupling to the grid is equal to unity and the blade pitch angle is $\beta = 0°$.

Fig. 4(a) and (b) validates that, for any given wind speed, LM in the DFIG and MPPT in the wind turbine can be achieved by properly controlling the q-axis output voltage $V_{q\mathrm{Cov}}$ of the GrSC and the q-axis rotor current I_{qr} of the DFIG, respectively.

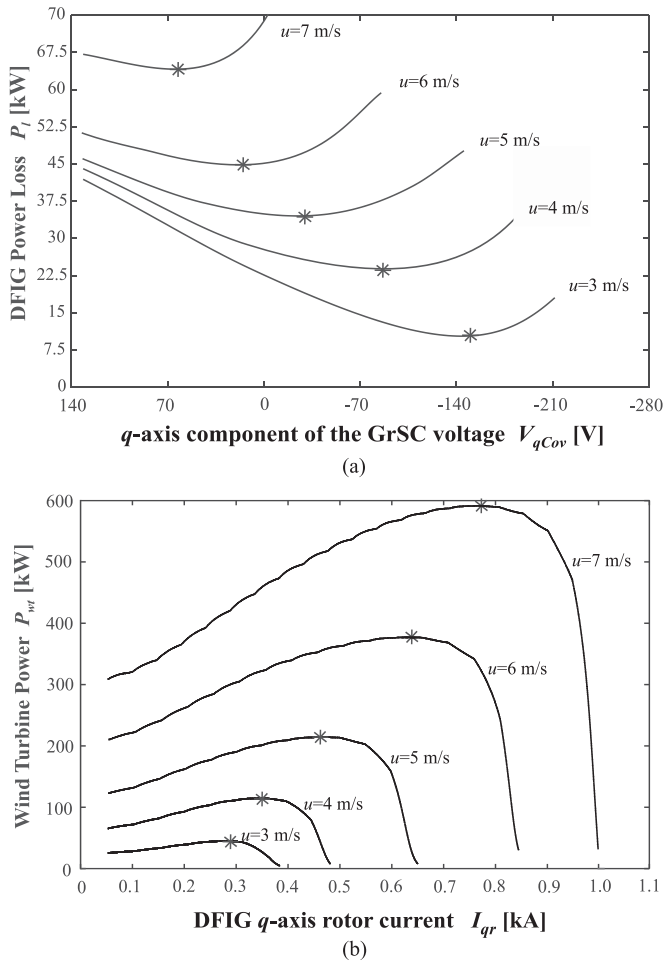

Fig. 4. Simulation results from a 1.6-MW WECS with DFIG of the variation of (a) DFIG power loss versus $V_{q\mathrm{Con}}$ voltage of the GrSC, for several wind speeds, while the rotor speed is manually adjusted for attaining MPP in the turbine and (b) wind turbine power versus I_{qr} current of the DFIG, for several wind speeds and for nominal stator voltage.

TABLE II
THREE-PHASE, 1.6-MW, WECS WITH DFIG

3-blades horizontal axis wind turbine:
C_p= 0.435 (max) for tip speed ratio (TSR) λ= 6.2
Blades Radius= 45 m Gear-Ratio= 1:120
3-phase DFIG:
V_s= 575 V (L-L, rms) I_s= 2010 A (rms)
f_e= 60 Hz $2p$= 6 (number of poles)
R_s= 1.45 mOhm R'_r= 0.992 mOhm J = 1065 Kg m^2
L_m= 1.5 mH L_{ls}= 0.09 mH L'_{lr}= 0.082 mH
c_{Fe_s}= 0.055 c_{Fe_r}= 0.055 c_{str}= 6•10^{-9}
Rotor transformer:
n_R= 1:1 150/150 V (L-L, rms) 750 kW L_m= 0.038 H
$R_1 = R'_2$= 1.4 mOhm $L_{l1} = L'_{l2}$= 1.2 μH
Grid transformer:
n_G= 1:1 400/400 V (L-L, rms) 1.8 MW L_m= 0.035 H
$R_1 = R'_2$= 1.2 mOhm $L_{l1} = L'_{l2}$= 1.1 μH
LCL filter:
R= 0.6 mOhm L = 2.8 μH C = 20 μF
Optimal controllers:
G_s= 2.41•10^{-3} G_r= 0.071
T_A= 1.56•10^{-6} T_B= 8.32•10^{-5} T_C= 8.32•10^{-5}

TABLE III
THREE-PHASE, 5.5-MW, WECS WITH DFIG

3-blades horizontal axis wind turbine:
C_p= 0.48 (max) for tip speed ratio (TSR) λ= 8
Blades Radius= 3 m Gear-Ratio= 1:10
3-phase DFIG:
V_s= 400 V (L-L, rms) I_s= 9.6 A (rms)
f_e= 50 Hz $2p$= 4 (number of poles)
R_s= 0.8 Ohm R'_r= 0.7 Ohm J = 0.1 Kg m^2
L_m= 0.38 H L_{ls}= 0.02 H L'_{lr}= 0.02 H
c_{Fe_s}= 8.62•10^{-5} c_{Fe_r}= 1.35•10^{-3} c_{str}= 4.5•10^{-6}
Rotor transformer:
n_R= 1:1 120/120 V (L-L, rms) 2.5 kW L_m= 0.6 H
$R_1 = R'_2$= 0.24 Ohm $L_{l1} = L'_{l2}$= 0.025 H
Grid transformer:
n_G= 0.7:1 285/400 V (L-L, rms) 7 kW L_m= 0.75 H
$R_1 = R'_2$= 0.26 Ohm $L_{l1} = L'_{l2}$= 0.03 H
LCL filter:
R= 0.065 Ohm L= 2 mH C = 35 μF
Optimal controllers:
G_s= 0.57 G_r= 6.2•10^{-3}
T_A= 1.9•10^{-6} T_B= 1.18•10^{-5} T_C= 1.85•10^{-4}

Specifically, Fig. 3(a) illustrates the variation of DFIG power loss P_l versus $V_{q\mathrm{Cov}}$ voltage for several wind speeds, while the rotor speed is manually adjusted for attaining MPP in the turbine. Fig. 3(b) shows the variation of the wind turbine power P_{wt} versus I_{qr} current, for several wind speeds and for nominal stator voltage in the DFIG. As can be seen, for each wind speed, there is an exact set of $V_{q\mathrm{Cov}}$ and I_{qr} values that provide LM in the DFIG and MPP in the turbine, respectively (points noted by asterisk).

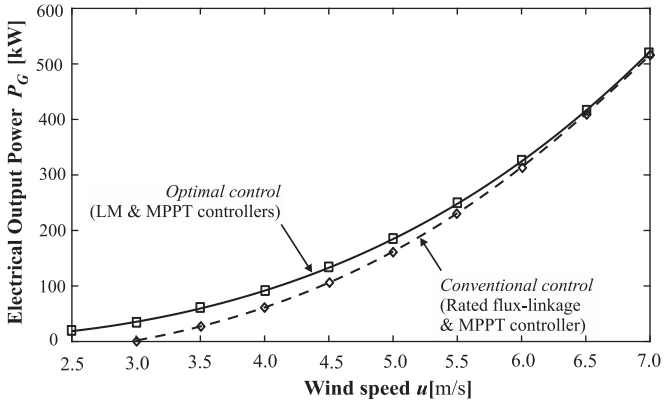

Fig. 5. Comparison in the generated electrical output power of the optimal efficiency against the conventional controlled WECS with DFIG (simulation results from a 1.6-MW wind system).

Fig. 5 compares the energy produced to the grid when both LM and MPPT optimal controllers are in operation (solid curve), against the case that only the MPPT controller is active and the DFIG operates with nominal stator voltage (dashed curve). The diagrams are extended up to wind speed of 7 m/s because this is the region with the more common wind energy potential [41]. As can be seen, the generated power is increased with the optimal-controlled WECS and higher increase is achieved at low wind speeds because higher reduction in the power loss can be accomplished. Moreover, the optimal-controlled WECS starts to provide energy to the grid from a wind speed lower than 2.5 m/s against the 3 m/s of the conventional system. Therefore, extension of the exploitable wind speed range toward the lower wind speed region is attained. As the wind speed increases, the flux-weakening margin is reduced and, consequently, the increase in the generated electric energy is reduced, too. From the nominal up to the rated wind speed, the DFIG operates with flux-linkage equal to the nominal.

It should be noted that the exact reduction of the cut-in wind speed and the increase in the electric power generation depend on the technical characteristics of the WECS. However, the proposed technique can attain maximum electric power generation and, more importantly, the power increase is higher at the low wind speed range which is usually the average wind energy potential. Furthermore, due to the reduction of the cut-in wind speed, the undesirable start-up and shutdown of the wind turbine, which are mainly attained at low wind speed range, are confined. Therefore, the WECS is longer in operation and the idle periods between successive start-up and shutdown are reduced, resulting in further increase of the generated power.

Fig. 6 illustrates the response of the LM optimal controller in a constant wind speed of 3.5 m/s, while the MPPT controller is active in all the simulation period. As can be seen, when the LM controller is energized at 12 s, the system reacts fast and finds the optimal efficiency operating point of the DFIG that corresponds to phase stator voltage 140 V rms, in less than 2 s. It is worth noting that, although the I_{qr} current is increased that results increase in the copper loss, considerable reduction of the iron loss is attained by the reduction of the airgap flux-linkage. Therefore, a correct balance is attained between copper,

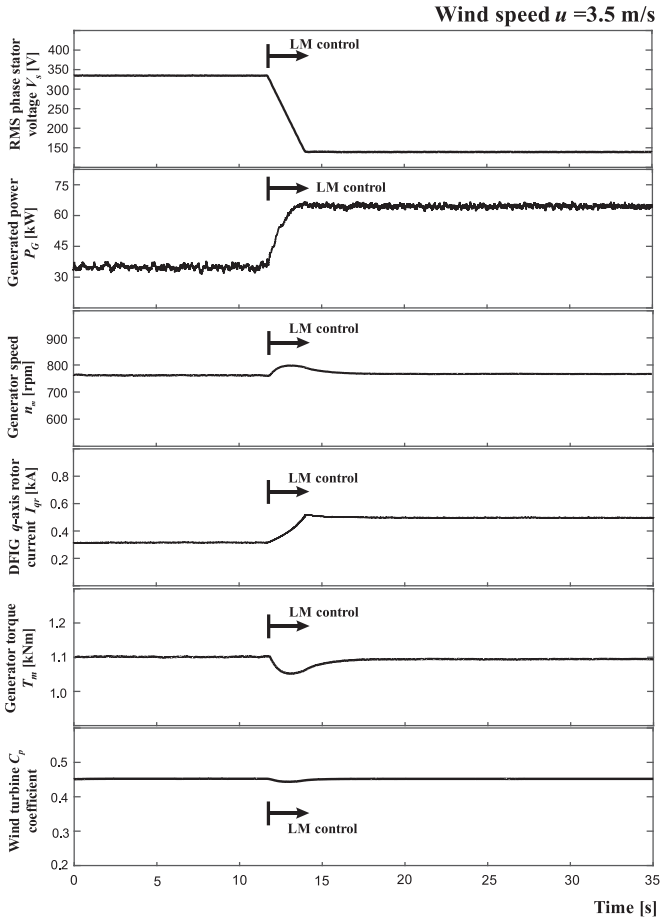

Fig. 6. Simulation results of the LM controller response in a 1.6-MW WECS. The LM controller is activated at $t = 12$ s, while the MPPT controller is in operation for all the simulation period.

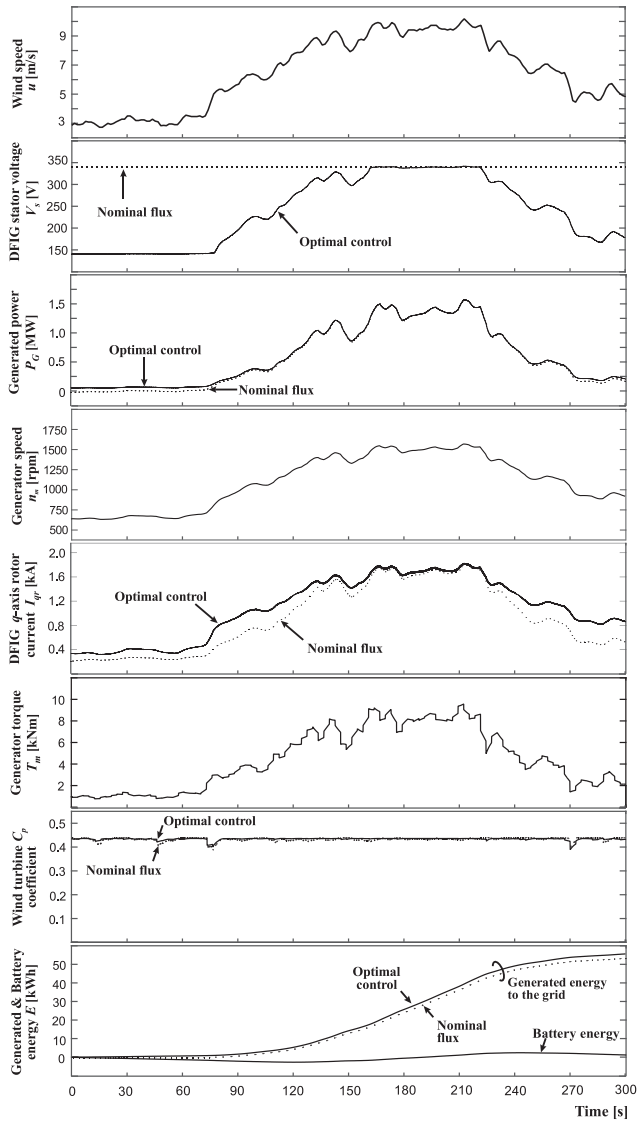

Fig. 7. Simulation results of the optimal efficiency controlled 1.6-MW WECS with DFIG (solid curves, both LM and MPPT controllers are in operation) against the conventional controlled (dotted curves, MPPT in the turbine and nominal stator flux in the DFIG), for a real wind speed profile obtained by measurements.

iron, and stray loss for minimizing the DFIG electrical loss and, consequently, 30 kW is additionally provided to the grid. The aerodynamic coefficient C_p of the wind turbine is almost constant equal to the maximum value 0.435 that is accomplished by the MPPT controller through the q-axis rotor current control.

Fig. 7 illustrates the performance of the optimal efficiency controlled WECS with DFIG in real wind speed conditions. The solid curves correspond to optimal efficiency operation and the dotted curves refer to the conventional control (MPPT with nominal stator voltage). As can be seen, the LM and MPPT optimal controllers satisfactorily follow the wind speed variations and additional 2.7 kWh is provided to the grid in the examined period of 5 min, through the LM in the DFIG. If the above rate of the additional generated energy is referred for a period of one year (since the examined wind speed profile is representative for the vast majority of wind applications), the annual additional energy that is provided to the grid with the proposed optimal efficiency control method is 280 MWh.

The energy that has been temporarily stored in the battery at the end of the examined period of 5 min is 0.5 kWh. This is to assist the operation of the GrSC to keep constant the dc-link voltage and also to provide energy and power smoothing against the wind speed variations. Thus, depending on the sign of the $V_{q\mathrm{Cov}}$, the battery may absorb or release electric energy. Specifically, if $V_{q\mathrm{Cov}}$ is positive, the battery operates in charging mode, while it turns to discharge mode when $V_{q\mathrm{Cov}}$ becomes negative.

Note that, if the WECS operation is continued beyond the examined 5 min, additional electric energy may be released or stored in the battery depending on the wind energy conditions. However, if a very long period of low wind speeds might occur (for example, more than 60 min for wind speeds below 3 m/s), the LM controller should be deactivated for some minutes and the WECS will operate with nominal flux, in order to protect the battery from complete discharge. During that period, the battery will be charged by part of the energy generated by the stator that flows to the GrSC through the common primary winding of the grid transformer, and when a satisfactory state of charge in the battery is accomplished, the WECS operation will return to

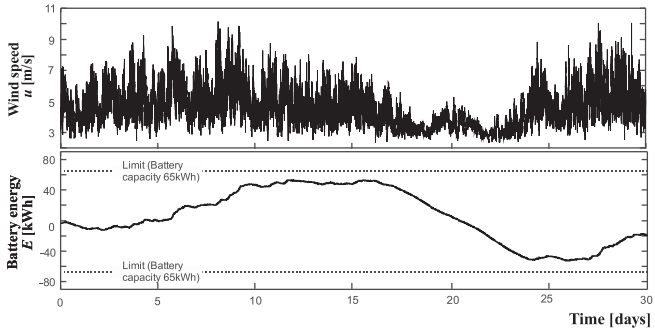

Fig. 8. Simulation results of the battery energy variation of the optimal efficiency controlled 1.6-MW WECS with DFIG for a period of one month, for a real wind speed profile obtained by measurements.

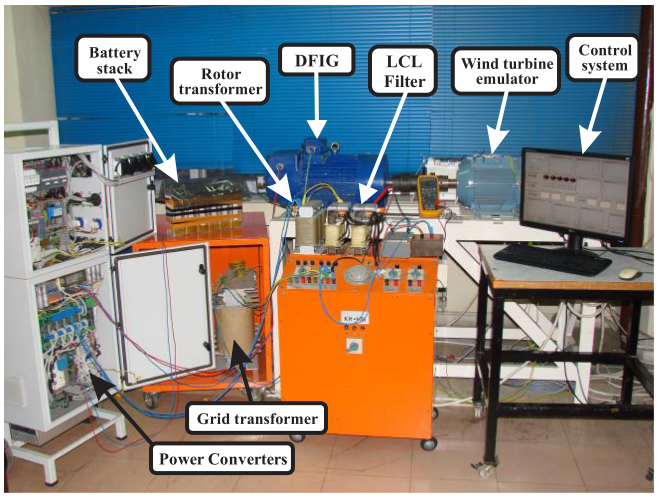

Fig. 9. Layout of a laboratory emulator WECS with a 5.5-kW DFIG that has been used for the experimental validation of the proposed optimal efficiency control scheme.

the optimal efficiency control. On the other hand, if the WECS operates for a long period with high wind speeds (for example, wind speeds above 9.5 m/s for more than 60 min) and the battery state of charge comes close to the maximum value, I_{qr} should be slightly decreased in order to turn the battery operation in discharging mode. Then, when the state of charge of the battery decrease to a satisfactory level, the WECS operation can again return to the optimal efficiency control.

The size of the Li-ion battery stack is 65 kWh (that corresponds to a battery pack of 70 Ah) and it is determined by considering the energy storage requirements of the WECS with DFIG in terms of power and energy capacity as well as economic objectives against the cost of the battery, as per [42]. The study is conducted for a period of one month so as to be more certain of the results. Fig. 8 illustrates the variation of the energy storage in the battery pack for a wind speed profile obtained by measurements. As it is observed, the maximum amount of the charged/discharged energy is within the limits of the battery energy storage capacity of 65 kWh. The utilization cost of the battery can be calculated by the following formula:

$$U_t = abs\left(aE_{\text{total}} - \beta E_{\text{bat,nom}}\right) \tag{42}$$

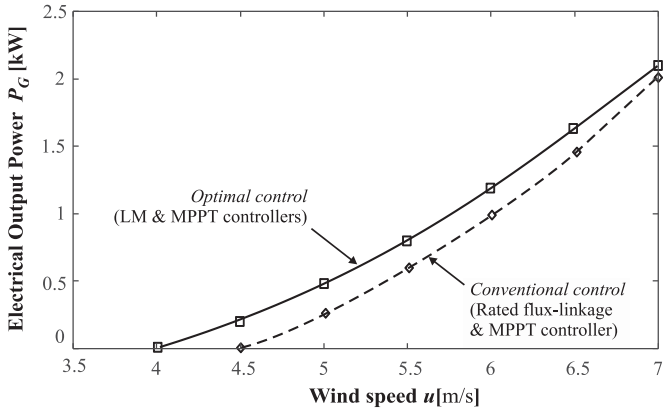

Fig. 10. Comparison in the generated electrical output power of the optimal efficiency against the conventional controlled WECS with DFIG (experimental results from a 5.5-kW wind system).

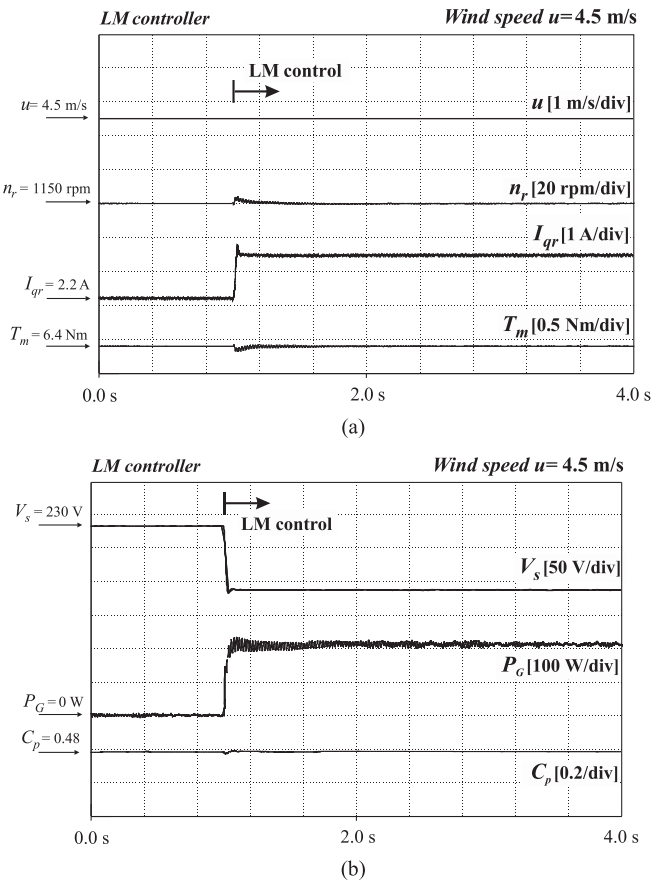

Fig. 11. Experimental results of the LM controller response in a 5.5-kW WECS with DFIG. The LM controller is activated at $t = 1$ s, while the MPPT controller is in operation for all the examined period.

where E_{total} is the total energy charged/discharged in the battery for the examined period, $E_{\text{bat,nom}}$ is the battery energy capacity, a is the price of the wind energy sold to the grid (€/kWh), and β is the amortized battery capital cost per hour (€/kWh/h). For the calculations, a = 0.08 €/kWh and $\beta = 0.0228$ €/kWh/h have been considered that are determined by taking into account that the battery cost is 500 €/kWh and, with a conservative assumption, the battery life is 2.5 years. From the above and

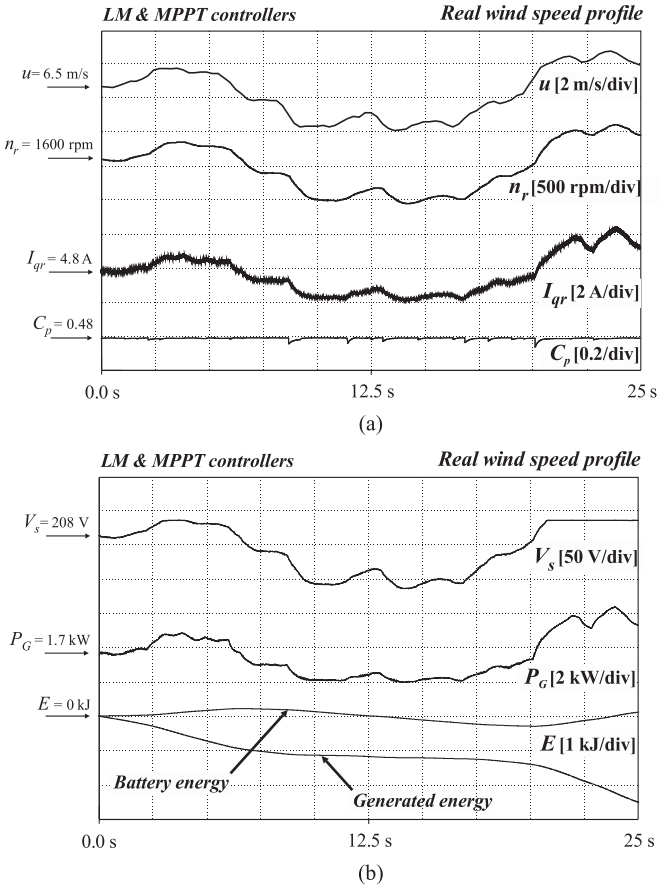

Fig. 12. Experimental results of the optimal efficiency 5.5-kW WECS with DFIG, for a real wind speed profile obtained by measurements (both LM and MPPT controllers are in operation).

considering that $E_{\text{total}} = 13$ MWh (it is obtained by integrating the battery energy E of Fig. 8 for the examined period), the utilization cost U_t is almost zero for selecting battery capacity of 65 kWh.

VII. Experimental Results

For the experimental validation of the proposed optimal efficiency control scheme, a 5.5-kW DFIG with a laboratory emulator wind turbine that utilizes an induction motor drive is used (see Fig. 9), as per [43]. The parameters of the WECS, DFIG, the rotor and grid transformers, the *LCL* filter, and the optimal controllers are reported in Table III.

Two dSPACE DS1104 controller boards are used for the implementation of the control system. The GeSC controller board houses the MPPT controller and the GrSC controller board houses the LM controller. The field-oriented control with space vector modulation is applied in the two back-to-back converters of the rotor side DFIG. A Li-ion battery stack with rated capacity of 2.5 A driven by a dc–dc converter is installed at the dc-link. The power factor at the point of common coupling to the grid is equal to unity and the blade pitch angle is $\beta = 0^{\circ}$.

As for the simulation analysis, Fig. 10 illustrates experimental results of the comparison between the optimal efficiency against the conventional controlled WECS. As can be seen, the generated power is increased with the optimal efficiency control method and the cut-in wind speed is reduced to 4 m/s against the 4.5 m/s of the conventional system.

Fig. 11 shows the performance of the LM controller for constant wind speed 4.5 m/s when the MPPT controller is in operation in all the examined period. As can be seen, the generated power has been increased by 210 W with the optimal efficiency controlled method.

Finally, Fig. 12 verifies the effectiveness of the optimal efficiency WECS in real wind speed conditions. As can be seen, the LM and MPPT optimal controllers satisfactorily cooperate for providing maximum efficiency in the DFIG and maximum power harvesting of the wind turbine and, therefore, optimal efficiency in the whole WECS.

VIII. Conclusion

In this paper, an optimal efficiency control scheme for a WECS with DFIG was presented, that provides LM in the electric generator and MPPT in the wind turbine. Therefore, increase in the generated electric energy for the same wind energy potential is achieved. Additionally, extension of the exploitable wind speed range toward the lower speed region is accomplished. The LM is based on the flux-weakening technique realized by the proper control of the output voltage of the rotor side grid converter and the MPPT is accomplished by regulating the rotor speed through the q-axis rotor current in the rotor side generator converter. An experimental procedure for determining the controllers' parameters has been presented and, therefore, the knowledge of the WECS model is not required. For the implementation of the optimal efficiency control system, a new structure of the WECS has been adopted, but the cost has not been considerably affected compared to the conventional system. The functionality and effectiveness of the proposed control scheme have been validated with several simulation and experimental results.

References

[1] S. Seman, J. Niiranen, S. Kanerva, A. Arkkio, and J. Saitz, "Performance study of a doubly fed wind-power induction generator under network disturbances," *IEEE Trans. Energy Convers.*, vol. 21, no. 4, pp. 883–890, Dec. 2006.

[2] P. Zhou, Y. He, and D. Sun, "Improved direct power control of a DFIG-based wind turbine during network unbalance," *IEEE Trans. Power Electron.*, vol. 24, no. 11, pp. 2465–2474, Nov. 2009.

[3] E. Hau, *Wind Turbines, Fundamentals, Technologies, Application, Economics*. Berlin, Germany: Springer-Verlag, 2013.

[4] T. Lei, M. Barnes, and M. Ozakturk, "Doubly-fed induction generator wind turbine modeling for detailed electromagnetic system studies," *IET Renew. Energy Gener.*, vol. 7, no. 2, pp. 180–189, 2013.

[5] Y.M. You, T.A. Lipo, and B. Kwon, "Optimal design of a grid-connected-to-rotor type doubly fed induction generator for wind turbine systems," *IEEE Trans. Magn.*, vol. 48, no. 11, pp. 3124–2137, Nov. 2012.

[6] J. Hu and Y. He, "Reinforced control and operation of DFIG-based wind power generation system under unbalanced grid voltage conditions," *IEEE Trans. Energy Convers.*, vol. 24, no. 4, pp. 905–915, Dec. 2009.

[7] G. Tapia and A. Tapia, "Wind generation optimization algorithms for a doubly fed induction generator," *IEE Proc.—Gener., Transmiss. Distrib.*, vol. 152, no. 2, pp. 253–263, Mar. 2005.

[8] L. Yang, G. Y. Yang, Z. Xu, Z. Y. Dong, K. P. Wong, and X. Ma, "Optimal controller design of a doubly-fed induction generator wind turbine system for small signal stability enhancement," *IET Gener., Transmiss. Distrib.*, vol. 4, no. 5, pp. 579–597, May 2010.

[9] A. Mesemanolis, C. Mademlis, and I. Kioskeridis, "Optimal efficiency control strategy in wind energy conversion system with induction generator," *IEEE Trans. Emerg. Sel. Topics Power Electron.*, vol. 1, no. 4, pp. 238–246, Dec. 2013.
[10] A. M. A. Amin, M. I. El Korfally, A. A. Sayed, and O. T. M. Hegazy, "Efficiency optimization of two-asymmetrical-winding induction motor based on swarm intelligence," *IEEE Trans. Energy Convers.*, vol. 24, no. 1, pp. 12–20, Jan. 2009.
[11] F. J. T. E. Ferreira, G. Baoming, and A. T. de Almeida, "Stator winding connection-mode management in line-start permanent magnet motors to improve their efficiency and power factor," *IEEE Trans. Energy Convers.*, vol. 28, no. 3, pp. 523–534, Mar. 2013.
[12] A. O. D. Tommaso, R. Miceli, G. R. Galluzzo, and M. Trapanese, "Efficiency maximization of permanent magnet synchronous generators coupled to wind turbines," in *Proc. IEEE Power Electron. Spec. Conf.*, 2007, pp. 1267–1272.
[13] A. Gensior, T. M. P. Nguyen, J. Rudolph, and H. Güldner, "Flatness-based loss optimization and control of a doubly fed induction generator system," *IEEE Trans. Control Syst. Technol.*, vol. 19, no. 6, pp. 1457–1466, Nov. 2011.
[14] Y. T. Weng and Y. Y. Hsu, "Sliding mode regulator for maximum power tracking and copper loss minimization of a doubly fed induction generator," *IET Renew. Power Gener.*, vol. 9, no. 4, pp. 297–305, 2015.
[15] Y. Tang, P. Ju, H. He, C. Qin, and F. Wu, "Optimized control of DFIG-based wind generation using sensitivity analysis and particle warm optimization," *IEEE Trans. Smart Grid*, vol. 4, no. 1, pp. 509–520, Mar. 2013.
[16] B. A. Chen, T. K. Lu, Y. Y. Hsu, W. L. Chen, and Z. C. Lee, "An analytical approach to maximum power tracking and loss minimization of a doubly fed induction generator considering core loss," *IEEE Trans. Energy Convers.*, vol. 27, no. 2, pp. 449–456, Jun. 2012.
[17] A. G. Abo-Khalil, H. G. Park, D. C. Lee, S. P. Ryu, and S. H. Lee, "Loss minimization control for doubly-fed induction generators in variable speed wind turbines," in *Proc. Int. Conf. IEEE Ind. Electron. Soc.*, Nov. 2007, pp. 1109–1114.
[18] B. Zhang, W. Hu, and Z. Chen, "Loss minimization operation of doubly fed induction generator based wind generation systems considering reactive power provision," in *Proc. Int. Conf. IEEE Ind. Electron. Soc.*, Nov. 2014, pp. 2146–2152.
[19] A. Balogun, O. Ojo, and F. Okafor, "Efficiency optimization of doubly-fed induction generator transitioning into shorted-stator mode for extended low wind speed application," in *Proc. Int. Conf. IEEE Ind. Electron. Soc.*, Nov. 2013, pp. 1601–1606.
[20] A. S. Helmy, A. Shaltout, and N. Abdel-Rahim, "Improving the efficiency of a doubly-fed induction generator in variable speed wind turbines under different modes of operation considering core loss," in *Proc. IEEE Int. Conf. Smart Energy Grid Eng.*, 2015, pp. 1–8.
[21] K. Krajangpan, W. Sadara, and B. Neammanee, "Control strategies for maximum active power and minimum copper loss of doubly fed induction generator in wind turbine system," in *Proc. IEEE Int. Conf. Power Syst. Technol.*, 2010, pp. 1–7.
[22] G. D. Marques and M. F. Iacchetti, "Field-weakening control for efficiency optimization in a DFIG connected to a DC-link," *IEEE Trans. Ind. Electron.*, vol. 63, no. 6, pp. 3409–3419, Jun. 2016.
[23] S. Mondal and D. Kastha, "Maximum active and reactive power capability of a matrix converter-fed DFIG-based wind energy conversion system," *IEEE J. Emerg. Sel. Topics Power Electron.*, vol. 5, no. 3, pp. 1322–1333, Sep. 2017.
[24] N. Karakasis, N. Jabbour, E. Tsioumas, and C. Mademlis, "Efficiency increase in a wind system with doubly fed induction generator," in *Proc. Int. Conf. IEEE Ind. Electron. Soc.*, Oct. 2016, pp. 1–6.
[25] I. John and B. Jayanand, "Voltage control and maximum power tracking of DFIG based wind power generator," in *Proc. IEEE Int. Conf. Power, Instrum., Control Comput.*, 2015, pp. 1–6.
[26] N. David and D. C. Aliprantis, "Improved efficiency of DFIG wind energy conversion systems by operating in the rotor-tied configuration," in *Proc. Int. Conf. Electr. Mach.*, Sep. 2014, pp. 189–195.
[27] F. Fateh, W. N. White, and D. Gruenbacher, "A maximum power tracking technique for grid-connected DFIG-based wind turbines," *IEEE J. Emerg. Sel. Topics Power Electron.*, vol. 53, no. 4, pp. 957–966, Dec. 2015.
[28] C. H. Liu and Y. Y. Hsu, "Effect of rotor excitation voltage on steady-state stability and maximum output power of a doubly fed induction generator," *IEEE Trans. Ind. Electron.*, vol. 58, no. 4, pp. 1096–1109, Apr. 2011.
[29] G. Pannell, D. J. Atkinson, and B. Zahawi, "Minimum-threshold crowbar for a fault-ride-through grid-code-compliant DFIG wind turbine," *IEEE Trans. Energy Convers.*, vol. 25, no. 3, pp. 750–759, Sep. 2010.
[30] D. Zhou, F. Blaabjerg, T. Franke, M. Tonnes, and M. Lau, "Reduced cost of reactive power in doubly fed induction generator wind turbine system with optimized grid filter," *IEEE Trans. Power Electron.*, vol. 30, no. 10, pp. 5581–5590, Oct. 2015.
[31] Y. Song and F. Blaabjerg, "Overview of DFIG-based wind power system resonances under weak networks," *IEEE Trans. Power Electron.*, vol. 32, no. 6, pp. 4370–4394, Jun. 2017.
[32] S. J. Chapman, *Electric Machinery Fundamentals*, 4th ed. New York, NY, USA: McGraw Hill, 2005.
[33] S. M. Muyeen, *Wind Energy Conversion Systems: Technology and Trends*. New York, NY, USA: Springer, 2012.
[34] E. Koutroulis and K. Kalaitzakis, "Design of a maximum power tracking system for wind-energy-conversion applications," *IEEE Trans. Ind. Electron.*, vol. 53, no. 2, pp. 486–494, Apr. 2006.
[35] M. Pucci and M. Cirrincione, "Neural MPPT control of generators with induction machines without speed sensors," *IEEE Trans. Ind. Electron.*, vol. 58, no. 1, pp. 37–47, Jan. 2011.
[36] R. M. Hilloowala and A. M. Sharaf, "A rule-based fuzzy logic con-troller for a PWM inverter in a stand-alone wind energy conversion scheme," *IEEE Trans. Ind. Appl.*, vol. 32, no. 1, pp. 57–65, Jan./Feb. 1996.
[37] A. C. Smith, R. Todd, M. Barnes, and P. J. Tavner, "Improved energy conversion for doubly fed wind generators," *IEEE Trans. Ind. Appl.*, vol. 42, no. 6, pp. 1421–1428, Nov./Sep. 2006.
[38] M. Z. Sujod, I. Erlich, and S. Engelhardt, "Improving the reactive power capability of the DFIG-based wind turbine during operation around the synchronous speed," *IEEE Trans. Energy Convers.*, vol. 28, no. 3, pp. 736–745, Sep. 2013.
[39] A. Mesemanolis and C. Mademlis, "Self-tuning maximum power point tracking control for wind generation systems," in *Proc. Int. Conf. Clean Electr. Power*, Jun. 2013, pp. 442–448.
[40] MATLAB/Simulink. Wind turbine doubly-fed induction generator (Phasor type). [Online]. Available: https://www.mathworks.com/help/physmod/sps/powersys/ref/windturbinedoublyfedinductiongeneratorphasortype.html
[41] F. D. Bianchi, H. De Battista, and R. J. Mantz, *Wind Turbine Control Systems, Principles, Modelling and Gain Scheduling Design*. London, U.K.: Springer-Verlag, 2007.
[42] X. Y. Wang, D. M. Vilathgamuwa, and S. S. Choi, "Determination of battery storage capacity in energy buffer for wind farm," *IEEE Trans. Energ. Convers.*, vol. 23, no. 3, pp. 868–878, Sep. 2008.
[43] N. Karakasis, A. Mesemanolis, and C. Mademlis, "Wind turbine simulator for laboratory testing of a wind energy conversion drive train," in *Proc. Int. Conf. MedPower*, 2010, pp. 1–6.

Nektarios Karakasis was born in Thessaloniki, Greece, on January 12, 1989. He received the Diploma degree from the School of Electrical and Computer Engineering, Aristotle University of Thessaloniki, Thessaloniki, Greece, in 2011, where he is currently working toward the Ph.D. degree in the area of energy management optimization in microgrids.

His research interests include the areas of energy efficiency optimization in wind systems, electric motor drives, power electronics and embedded systems design.

Evangelos Tsioumas was born in Kompotades Fthiotidas, Greece, on June 13, 1988. He received the Diploma degree from the School of Electrical and Computer Engineering, Aristotle University of Thessaloniki, Thessaloniki, Greece, in 2013, where he is currently working toward the Ph.D. degree in the area of energy management optimization in microgrids.

His research interests include energy management in power systems, control optimization in microgrids, large-scale electric energy storage systems, and embedded systems design.

Nikolaos Jabbour was born in Thessaloniki, Greece, on December 4, 1988. He received the Diploma degree in 2012 from the School of Electrical and Computer Engineering, Aristotle University of Thessaloniki, Thessaloniki, Greece, where he is currently working toward the Ph.D. degree in the area of control system optimization.

His research interests include control optimization, electrical machines and drives, power electronics, renewable energy systems, and embedded systems.

Ali M. Bazzi (S'07–M'10–SM'17) received the B.E. and M.E. degrees in electrical engineering from the American University of Beirut, Beirut, Lebanon, in 2006 and 2007, respectively. He received the Ph.D. degree from the University of Illinois at Urbana-Champaign (UIUC), Urbana, IL, USA, in 2010.

He joined the Department of Electrical and Computer Engineering, University of Connecticut, Storrs, CT, USA, in 2012, as an Assistant Professor where he established and currently directs the Advanced Power Electronics and Electric Drives Laboratory. He was a Senior Power Electronics Electrical Engineer with Delphi Electronics and Safety during 2011–2012, a visiting Assistant Professor with UIUC during spring 2011, an Engineer with Bitrode Corporation in the summers of 2008 and 2009, and a Research and Teaching Assistant with UIUC between 2007 and 2010. In 2016, he became a UTC Assistant Professor for Engineering Innovation at UCONN. He has over 80 peer-reviewed and refereed technical publications. His research interests include power electronics design, control, optimization, fault diagnosis, and reliability modeling in motor drives, solar photovoltaics, and other applications. He is also interested in renewable energy integration in microgrids, and real-time control and optimization of energy systems in general.

Dr. Bazzi has served on the organizing and technical committees of many IEEE conferences. He received the Mavis Memorial Scholarship from UIUC in 2009, the Outstanding Teaching Award from the ECE Department at UCONN in 2014, and the Research Excellence Award from UCONN in 2015. He is a member of the IEEE Industry Applications Society, IEEE Power Electronics Society, IEEE Power and Energy Society, and IEEE Industrial Electronics Society.

Christos Mademlis (S'96–A'00–M'03–SM'11) was born in Arnea Chalkidikis, Greece, on February 7, 1964. He received the Diploma degree in electrical engineering (first class hons.) and the Ph.D. degree in electrical machines from the Aristotle University of Thessaloniki, Thessaloniki, Greece, in 1987 and 1997, respectively.

Since 1990, he has been with the Electrical Machines Laboratory, Faculty of Electrical and Computer Engineering, Aristotle University of Thessaloniki as Research Associate (1990–2001), a Lecturer (2001–2006), an Assistant Professor (2007–2014), and currently an Associate Professor (since 2014). During 2013–2016, he was the Head of the Department of Electrical Energy and since 2010, he has been the Director of the Electrical Machine Laboratory, Faculty of Engineering, Aristotle University of Thessaloniki. He was the founder and in 2013–2017 the Faculty Advisor of the Student Formula SAE racing team of the Aristotle University of Thessaloniki. His research interests include the areas of electrical machines and drives, especially in design and control optimization, renewable energy sources, energy saving systems and energy management in zero energy buildings.

In 2017, Dr. Mademlis was awarded a Fulbright Grant as a Visiting Professor at the APED, Electrical and Computer Engineering Department, University of Connecticut, Storr, CT, USA.